DEUTSCHES ELEKTRONEN-SYNCHROTRON DESY

DESY 86-094
August 1986

NEWEST RESULTS FROM THE EMC

by

F. Janata
II. Institut f. Experimentalphysik, Universität Hamburg

ISSN 0418-9833

NOTKESTRASSE 85 · 2 HAMBURG 52

To be sure that your preprints are promptly included in the
HIGH ENERGY PHYSICS INDEX ,
send them to the following address (if possible by air mail) :

DESY
Bibliothek
Notkestrasse 85
2 Hamburg 52
Germany

DESY 86-094

ISSN 0418-9833

NEWEST RESULTS FROM THE EMC*

FRIEDRICH JANATA

II. Institut für Experimentalphysik, Universität Hamburg
Luruper Chaussee 149, D-2000 Hamburg 50, FRG

ABSTRACT

The most recent results on hadron production from muon scattering off H_2 and D_2 targets are presented. The analyses of the EMC data discussed here deal with the determination of the quark distribution functions and the investigation of QCD effects in terms of jet profiles or the transverse momenta of hadrons. For a better understanding of the fragmentation process correlations are studied in detail and the production characteristics of various vector and tensor mesons are compared with each other.

1. INTRODUCTION

Charged lepton scattering is an ideal tool to study the basic concepts by which the partonic structure of matter (quark distribution functions), the strong interactions (QCD) and the hadronisation process (fragmentation models) can be described. The experimental data obtained by the 4π detector of EMC(NA9)[1] allow a very detailed investigation of the items just mentioned because of the large number of events recorded over a wide kinematical range combined with excellent particle identification and also the possibility to detect photons.

In this report the following variables are used: the event variables Q^2 (mass of the virtual photon squared), W (centre-of-mass energy of the hadronic final state) and the Bjorken scaling variable $x = Q^2/(2m\nu)$ (m: nucleon mass, ν: energy of the virtual photon in the laboratory). The hadrons are described by the longitudinal variables $x_F = 2p^*_{\parallel}/W$ (Feynman x), $y = \frac{1}{2}ln(\{E^* + p^*_{\parallel}\}/\{E^* - p^*_{\parallel}\})$ (rapidity) or $z = E/\nu$ (E^*, $p^*_{\parallel}$: energy and momentum parallel to the virtual photon direction in the cms, E: energy in the laboratory) and by $p_\perp$, the momentum perpendicular to the virtual photon direction.

*Talk given at the XVII International Symposium on Multiparticle Dynamics, Pamhagen, Austria, June 16-20 1986

2. QUARK DISTRIBUTION FUNCTIONS

The determination of quark distribution functions is usually based on the measurements of structure functions. In charged lepton scattering from protons or neutrons the structure functions F_2^p and F_2^n are, in the framework of the quark-parton model, given by

$$F_2^p(x) = \frac{4}{9}xu_V(x) + \frac{1}{9}xd_V(x) + xsea(x) \tag{1}$$

$$F_2^n(x) = \frac{1}{9}xu_V(x) + \frac{4}{9}xd_V(x) + xsea(x) \tag{2}$$

where u_V, d_V and sea denote the distribution functions of the valence u quarks, the valence d quarks and of the sea in the proton. In order to extract these distribution functions, appropriate parametrisations[2] of them in x and Q^2 are inserted into equations (1) and (2) which are then fitted to the measured structure functions. The fits may be constrained by the quark-parton model sum rules.

An alternative method was adopted by the EMC[3] which is based on the quark-parton model formula for hadron production

$$\frac{1}{N_\mu}\frac{dN^h}{dz} = \sum_i \frac{e_i^2 q_i(x)}{\sum_j e_j^2 q_j(x)} \cdot D_i^h(z) \tag{3}$$

where e_i and $q_i(x)$ are the quark charges and distribution functions and the sums run over all quarks and antiquarks. A kind of flavour tagging can be achieved since the contributions from the various quark flavours are different depending on the type of the hadron which is produced. If one assumes that only two kinds of fragmentation functions exist, namely favoured (the scattered quark is contained in the hadron) and unfavoured (the scattered quark is not contained in the hadron) fragmentation functions, and applying the usual isospin and charge conjugation relations among the fragmentation functions one gets (proton target)

$$\left(N^{\pi^+}(x) - N^{\pi^-}(x)\right)\Big|_p \equiv \frac{1}{N_\mu}\int_0^1 \left(\frac{dN^{\pi^+}}{dx_F} - \frac{dN^{\pi^-}}{dx_F}\right)dx_F = \frac{1}{9F_2^p(x)}[4xu_V(x) - xd_V(x)]\underbrace{\int_0^1 \left(D_u^{\pi^+}(x_F) - D_u^{\pi^-}(x_F)\right)dx_F}_{D^\pi} \tag{4}$$

and

$$\left(N^p(x) - N^{\bar{p}}(x)\right)\Big|_p = \frac{1}{9F_2^p(x)}[4xu_V(x) + xd_V(x)]D^p. \tag{5}$$

In the case of a deuterium target the analogues to formulae (4) and (5) are

$$\left(N^{\pi^+}(x) - N^{\pi^-}(x)\right)\Big|_{D_2} = \frac{1}{9F_2^{D_2}(x)}3[xu_V(x) + xd_V(x)]D^\pi \tag{6}$$

and

$$\left(N^p(x) - N^{\bar{p}}(x)\right)\Big|_{D_2} = \frac{1}{9F_2^{D_2}(x)} 5[xu_V(x) + xd_V(x)]D^p. \qquad (7)$$

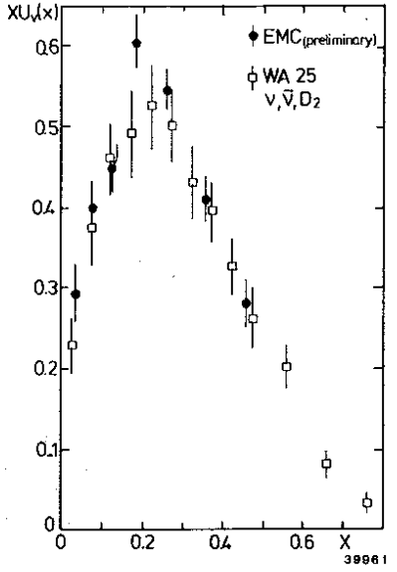

For $x \to 1$ the right hand sides of (6) and (7) approach $\frac{3}{5}D^\pi$ and D^p respectively. D^π and D^p are determined from fits of the functional form $D\frac{x^\alpha}{1-K(1-x)^\beta}$ to the left hand sides of equations (6) and (7) as determined by experiment. With the results of these fits and the parametrisations of F_2^p ($Q^2 = 18GeV^2$) from ref. 2 $xu_V(x)$ is extracted from the sum of equations (4) and (5) and shown in fig. 1. For comparison the results on $xu_V(x)$ derived from measurements of F_2 and F_3 in a $\nu(\overline{\nu})D_2$ scattering experiment[4] are also included in this figure. Good agreement between these two very different approaches can be observed.

Fig. 1: Distribution function for valence u quarks versus x.

3. QCD Effects

3.1 Jet Profiles

In the simple quark-parton model the fragmentation functions do not depend on any of the event variables but in leading and next to leading order QCD they are expected to acquire Q^2 (or W^2) and x dependences. In order to examine this effect the single particle distributions are studied in the forward and backward hemispheres in terms of jet profiles which are defined as

$$\frac{1}{N_\mu}\frac{d\varepsilon}{d\lambda} \quad \text{with} \quad \varepsilon = \frac{\sum_{\Delta\lambda} E^*}{\sum_{\lambda>0 \text{ or } \lambda<0} E^*} \quad \text{and} \quad \lambda = \frac{x_F}{p_\perp} = \frac{cot\theta^*}{W/2} \qquad (8)$$

where the sums run over the charged hadrons in a given λ interval (numerator) or the ones going into the forward (backward) hemisphere (denominator). θ^* is the angle between the hadron and the virtual photon in the cms.

Scale breaking is investigated[5] via ratios of jet profiles from different W ranges. The ratios are denoted by Wik, i and k being the numbers of the chosen W intervals (W1: 4-8GeV, W2: 8-12GeV, W3: 12-16GeV, W4: 16-20GeV). The

jet profiles which are obtained from a Monte-Carlo simulation based on the quark-parton model and independent fragmentation show scaling, i.e. the ratios Wik are almost equal to one and depend only very weakly on λ (dot-dashed lines in fig. 2). The data scale in the backward hemisphere but do not scale forward.

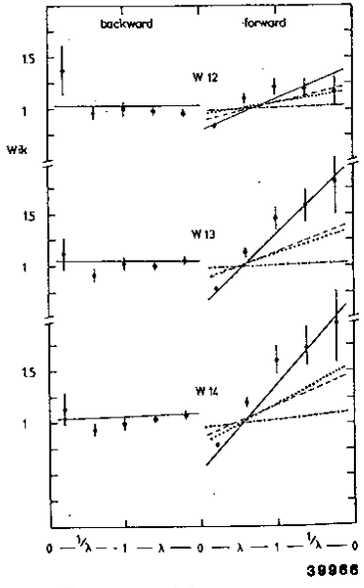

Such a forward-backward asymmetry is expected from soft QCD effects but not from fragmentation or from the influence of the primordial transverse momentum of the scattered quark. The complete Lund model (first order QCD graphs, string fragmentation and soft gluon effects) represents the data in a rather satisfactory way (solid lines) whereas omitting soft and hard QCD effects (dashed lines) leads to deviations from the experimental results. The model in which string fragmentation and soft gluon effects are replaced by independent fragmentation (dotted lines) is also not able to reproduce the experiment.

Fig. 2: Ratios of jet profiles in different W intervals as a function of λ. The data (circles) are compared with various model calculations which are represented by straight line fits and discussed in the text.

3.2 Transverse Momentum

In charged lepton scattering the transverse momentum is determined with respect to the virtual photon direction. To the observed $p_\perp$ several processes contribute. These contributions stem from the transverse momentum of the quark-antiquark pairs created in the fragmentation process, from the primordial transverse momentum of the scattered quark due to its Fermi motion in the target nucleon, from soft gluons which are too soft to fragment but give recoil to the leading quark and from hard gluon bremsstrahlung. All of these effects are incorporated in the Lund model. In fig. 3 it is demonstrated that all these four mechanisms are necessary to reproduce the experimental results[6] on $\langle p_\perp^2 \rangle$ versus x_F.

The contributions from hard QCD effects are especially important in order to explain the occurance of high $p_\perp$ particles. This can be shown best by comparing the distribution of $\sum(p_\perp^{in})^2$ ($p_\perp^{in}$: transverse momentum projected onto the plane in which the sum of all hadrons' $p_\perp$ is maximum) with various model calculations in analogy to those presented in fig. 3. The high $\sum(p_\perp^{in})^2$ tail can only be reproduced[7] if hard QCD processes are taken into account. It has also

been shown[7,8] that the independent fragmentation scheme is not able to reproduce the behaviour of $\langle p_\perp^2 \rangle$ at positive x_F, even if Λ_{QCD} is increased to the rather improbable value of 1 GeV.

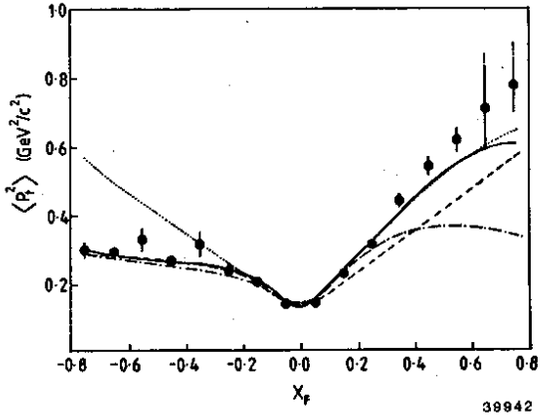

Fig. 3: Mean transverse momentum squared versus x_F. The circles represent the data and the curves various model predictions: standard Lund model (solid line), Lund model without hard QCD (dashed line), Lund model without soft gluons (dot-dashed line), Lund model without soft gluons but with increased primordial transverse momentum (dotted line).

4. FRAGMENTATION

4.1 Correlations

The study of correlations allows to gain a more detailed insight into the hadronisation process which is usually described by models since a coherent theory of fragmentation is still lacking. In most of these fragmentation models mesons are created via quark-antiquark pairs. The consequence of this picture is that neighbouring charged hadrons are expected to have opposite charges. To experimentally investigate this conjecture is not without problems since resonance decays and baryon production will dilute this clean picture somewhat. Furthermore, the choice of the variable in which one can expect to retain the original ordering of the hadrons is to some extent arbitrary (x_F or y are commonly used in this context). However it can be shown[9] that the observed charge correlations are largely due to the fragmentation process.

In fig. 4, R_1, the probability that hadrons which are adjacent in x_F have opposite charges, is presented[9,10] as a function of W^2. R_1 decreases with increasing W^2 but lies systematically above the corresponding values from the random charge model (RCM: Lund model but the charges are randomly redistributed among the

hadrons) which follows the same trend. This decrease can be explained by the rising charged hadron multiplicity[11] with W^2 which weakens the influence of the overall charge conservation on R_1. From the presence of a clear difference between the data and the RCM values, independent of W^2, one can conclude that the charge correlation observed is of a short range nature since the net effect is independent of W^2 and does therefore also not depend on the number of hadrons in an event.

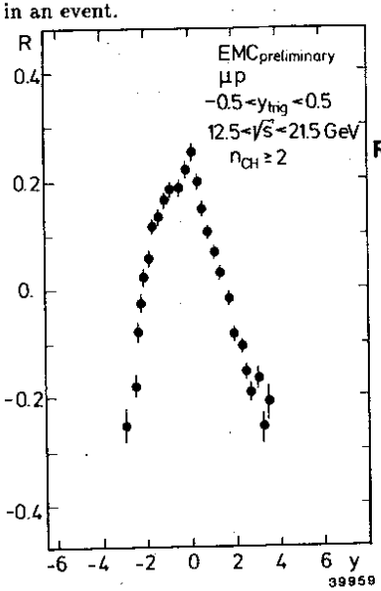

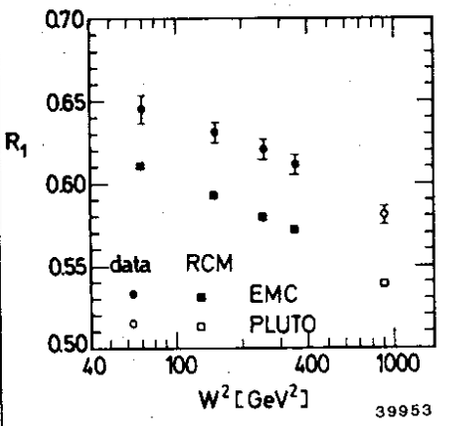

Fig. 4: Fraction of hadron pairs with opposite charges adjacent in x_F versus W^2.

Fig. 5: Correlation function $R(y_{trig}, y)$ for charged hadrons with $|y_{trig}| < 0.5$ vs. y.

Correlations between two particles (labelled with a and b) can be studied in terms of the normalized correlation function

$$R(y_1, y_2) = \frac{\rho_2^{ab}(y_1, y_2)}{f \rho_1^a(y_1) \rho_1^b(y_2)} - 1 \qquad (9)$$

with $\rho_1(y) = \frac{1}{N_\mu} \frac{dN}{dy}$ and $\rho_2(y_1, y_2) = \frac{1}{N_\mu} \frac{d^2N}{dy_1 dy_2}$ being the normalized one and two particle densities respectively. The normalisation factor f is chosen such that in the absence of correlations $R(y_1, y_2)$ is equal to zero.

The results on $R(y_1, y_2)$ from μp scattering[12] are shown in fig. 5 for the case of a central trigger interval. The correlation function is positive in the rapidity range around the trigger interval and becomes negative more than one unit of rapidity away. Qualitatively the same behaviour was also found in pp and e^+e^- reactions[13,14] but a quantitative comparison is difficult since the energies, the widths of the trigger intervals and the multiplicities of the three experiments are

very different. In the multichain dual model[15] one would expect the μp result to be rather similar to e^+e^- since in both cases only one string contributes to the production of the hadrons (for more details see discussion in ref. 13). However, before a meaningful comparison between μp scattering and e^+e^- annihilation can be performed the data must be analyzed under the same conditions.

The Bose-Einstein interference effect allows to analyze the space-time structure of the emission region of particles in high energy interactions. This effect is based on the interference between the wave functions of two identical bosons which are here chosen to be $\pi^+\pi^+$ and $\pi^-\pi^-$ pairs. The strength of the effect is most frequently parametrized by

$$I = 1 + \lambda e^{-\widetilde{M}^2 R^2} \quad (\text{with } \widetilde{M}^2 = M^2_{eff} - 4m^2_\pi) \tag{10}$$

where R is the size of the pion source and λ ($0 \leq \lambda \leq 1$) is the suppression factor describing the deviation from complete chaos ($\lambda = 1$).

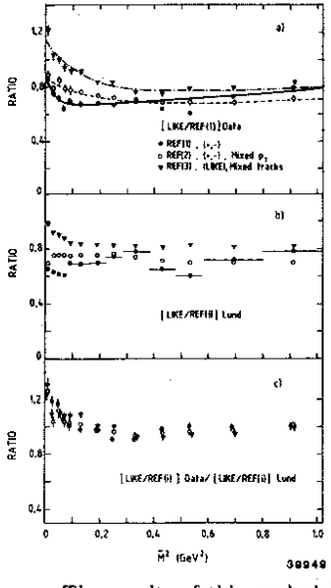

Fig. 6: The ratios of the $\widetilde{M}^2$ distibutions for like-sign pion pairs and three different reference samples for (a) the data and (b) the Lund model. In (c) the ratios of the corresponding ratios in (a) and (b) are given.

The most difficult part in the analysis of the Bose-Einstein effect is the choice of an appropriate reference sample by which the like sign pion pairs (denoted by LIKE) have to be normalized. The following three different methods have been adopted by the EMC:

REF(1): $\pi^+\pi^-$ pairs are taken from the same event,

REF(2): like REF(1) but the $p_\perp$ values are redistributed at random,

REF(3): $\pi\pi$ combinations are taken from different events with similar W values and equal multiplicities.

The results of this analysis[16] are shown in fig. 6. In fig. 6a the ratios of LIKE/REF(i) are given as a function of $\widetilde{M}^2$. The different reference samples lead to different results but this is also true for the Lund model (fig. 6b) which does not contain the Bose-Einstein effect. If one assumes that the influences of the reference samples are properly described by the Lund model and can be factorized out the double ratios shown in fig. 6c should be independent of the choice of the

reference sample. In good approximation this is indeed the case. By fitting the function (10), multiplied by $(1 + \delta\widetilde{M}^2)$ to account for the observed increase of the ratios with $\widetilde{M}^2$, to the points shown in fig. 6c the following results (table 1) are obtained which are compared with the results from e^+e^- annihilation[17,18].

Table 1: Parameters R and λ as obtained from fits to the double ratios (fig. 6c).

reference sample	R/fm(μp)	$\lambda(\mu p)$	R/fm(e^+e^-)
REF(1)	0.84±0.03	1.08±0.10	0.76±0.12 (TASSO)
REF(2)	0.66±0.01	0.60±0.06	
REF(3)	0.46±0.03	0.73±0.06	0.65±0.04±0.05 (TPC)

The size of the pion emission region is found to be of the order of 0.5-0.8fm, in agreement with the e^+e^- results. Differences between the longitudinal and transverse diameters of the source could not be established.

4.2 Production of Vector and Tensor Mesons

In addition to studies of inelastic ρ^0 production in μp scattering data on ω, $\phi(1020)$ an f(1270) are also available now[19,20,21]. They have been obtained via the following decays: $\omega \to \pi^+\pi^-\pi^0$, $\phi \to K^+K^-$, $f \to \pi^+\pi^-$. The reconstruction of ω and ϕ mesons became possible because of the lead glass detector (π^0) and the time-of-flight and Cerenkov counters ($K^\pm$) belonging to the EMC apparatus.

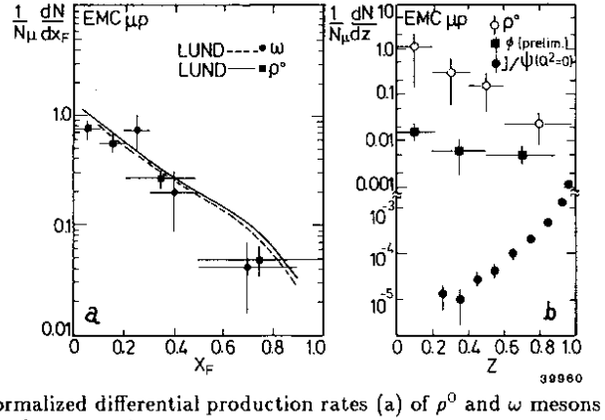

Fig. 7: Normalized differential production rates (a) of ρ^0 and ω mesons versus x_F and (b) of ρ^0, ϕ and J/Ψ mesons versus z.

The ρ^0 and ω yields agree with each other very well as expected (fig. 7a) and can be successfully described by the Lund model. ϕ production is less frequent and much flatter as a function of z than ρ^0 and ω production whereas J/Ψ production[22] (note the different Q^2 value) is even more suppressed and increases

towards $z = 1$. The differences shown in fig. 7b in the behaviour of vector mesons of different masses can be understood in the following way: at low z the mesons stem from the fragmentation process in which the creation of $s\bar{s}$ (ϕ) and $c\bar{c}$ (J/Ψ) pairs are strongly suppressed. At high z the vector mesons can be created diffractively and the coupling of the photon to s and c quarks is proportional to the squares of the quark charges. So the yields are expected not to differ by orders of magnitude in the high z region.

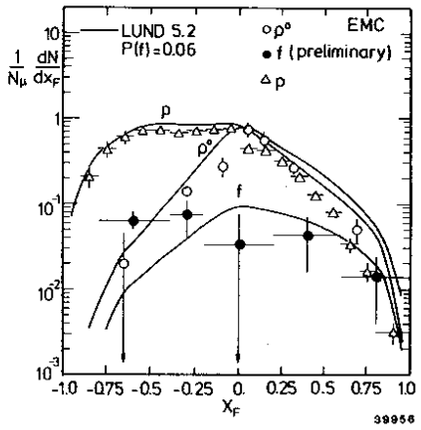

The production of the tensor meson f(1270) was measured by the EMC over almost the complete x_F range. The most striking feature (fig. 8) certainly is the rather weak dependence on x_F. The relatively high yield in the backward hemisphere is especially puzzling. A more detailed analysis of these still preliminary data is necessary till one can draw firm conclusions.

Fig. 8: Normalized differential production rate of f mesons as a function of x_F. Results on proton[23] and ρ^0 meson production are shown for comparison.

References

1. EMC, Albanese, J.P. et al., Nucl. Inst. Meth. **212**, 111 (1983).
2. EMC, Aubert, J.J. et al., Nucl. Phys. **B259**, 189 (1985).
3. EMC, Benchouk, Ch., Ph.D. Thesis, Univ. of Aix-Marseille-II (1986).
4. WA25 collaboration, Allasia, D. et al., Phys. Lett. **135B**, 231 (1984).
5. EMC, Berghoff, G., Talk at the XXI Recontre de Moriond, Les Arcs, France (March 1986).
6. EMC, Arneodo, M. et al., Phys. Lett. **149B**, 415 (1984).
7. EMC, Geddes, N., Ph.D. Thesis, Univ. of Oxford, preprint RAL T 017 (1985).
8. Renton, P., Talk at the XVI International Symposium on Multiparticle Dynamics, Kiryat-Anavim, Israel (June 1985).
9. EMC, Arneodo, M. et al., Z. Phys. **C31**, 333 (1986).
10. PLUTO collaboration, Berger, Ch. et al., Nucl. Phys. **B214**, 189 (1983).
11. EMC, Arneodo, M. et al., Nucl. Phys. **B258**, 249 (1985).
12. EMC, Krüger, J., Ph.D. Thesis, Univ. of Wuppertal, preprint WU B-DI 85-4 (1985).
13. TASSO collaboration, Althoff, M. et al., Z. Phys. **C29**, 347 (1985).
14. Breakstone, A. et al., Phys. Lett. **114B**, 383 (1982).
15. Capella, A., Proc. of the Europhysics Study Conference, Erice, Italy (1981).

16. EMC, Arneodo, M. et al., preprint CERN-EP/86-42 (1986).
17. TPC collaboration, Aihara, H. et al., Phys. Rev. **D31**, 996 (1985).
18. TASSO collaboration, Althoff, M. et al., Z. Phys. **C30**, 355 (1986).
19. EMC, Arneodo, M. et al., preprint CERN-EP/86-99 (1986).
20. EMC, Montanet, F., Ph.D. Thesis, Univ. of Aix-Marseille-II (1986).
21. EMC, Pötsch, M., Ph.D. Thesis, Univ. of Wuppertal (1986).
22. EMC, Aubert, J.J. et al., Nucl. Phys. **B213**, 1 (1983).
23. EMC, Arneodo, M. et al., Phys. Lett. **150B**, 458 (1985).